Morphogenesis of Evaporation-Induced Self-Assemblies of Polypyrrole Nanoparticles Dispersed in a Liquid Medium

Jyongsik Jang* and Joon Hak Oh

Hyperstructured Organic Materials Research Center and School of Chemical Engineering, Seoul National University, Shinlimdong 56-1, Seoul 151-742, Korea

Received March 22, 2004. In Final Form: August 2, 2004

Evaporation-induced self-assemblies (EISAs) with various morphologies were selectively fabricated by drying a solution containing polypyrrole nanoparticles. The morphogenesis of EISAs was strongly dependent upon the solvent evaporation rate and the nanoparticle concentration. In the case of fast evaporation, 2-D dendrites or pseudo 1-D dendrites were observed. When the liquid medium evaporated slowly, ring and spherulitic assemblies took place. Multiple rings could be created on a substrate surface under one single drop.

Introduction

There has been growing interest in the self-assemblies of semiconductor, metal, and metal oxide nanoparticles, because they usually show different electronic and optical properties from those of isolated nanoparticles. In the diverse methods to form self-assemblies of nanoparticles, one of the simplest approaches is to employ a liquid medium. During the evaporation process of the liquid medium, various self-assemblies of nanoparticles can be formed depending on the experimental conditions.[1−3]

Okubo and co-workers reported the formation of dissipative structures in the course of drying a colloidal solution and conducted rheological and kinetic analyses.[4−7] Shimomura et al. employed dissipative patterns formed by drying a polymer colloidal solution for mesoscopic patterning.[8,9] Gelbart et al. have demonstrated the mechanism of solvent dewetting in submonolayer annular arrays formed by drying organically passivated metal colloids on a substrate.[10−12] Brinker and co-workers developed evaporation-induced self-assemblies (EISAs) that enable the rapid production of patterned mesoporous and nanocomposite materials in the form of films, fibers, or powders.[13−15] Sommer and colleagues obtained circular deposition patterns in evaporating drops of polymer aqueous suspension.[16,17]

Although the formation of dissipative structures of colloidal particles during solvent evaporation has been well documented, the fabrication of diverse EISA morphologies from one suspension system has rarely been carried out. Furthermore, self-assemblies of organic latices have been largely prepared using colloids with dimensions larger than several tens of nanometers.

Herein, we report on the selective fabrication of various EISA morphologies including dendrites, ring patterns, and spherulitic structures from one polymer colloidal system. We describe the effect of the evaporation rate and nanoparticle concentration on the morphogenesis of EISAs. Polypyrrole (PPy) nanoparticles with diameters of several nanometers were employed to prepare a polymer suspension solution. This size range is much smaller than those of other polymer colloids studied in earlier reports, and thus highly developed organic EISA morphologies could be obtained within a small size domain.

Experimental Section

PPy nanoparticles with an average diameter of 5 nm were prepared by the method reported previously.[18,19] A variable amount of the PPy nanoparticles was dispersed in ethyl alcohol, and a drop (12 μL) of the solution was placed on a carbon grid (3.0 mm diameter) and allowed to evaporate. The margins of the drop coincided with the grid. A schematic drawing of the evaporation system is shown in Figure 1. We manufactured a Pyrex glass container. A vacuum was applied inside the container to enhance the adiabatic effect of the glass chamber. The volume of the container was about 1000 cm^3. The sample was placed on an adiabatic support. Small containers filled with silica gel were placed around the preparation zone to avoid high humidity originating from the evaporation process. The thermometer was tied up with adhesive tape. The gauge of the temperature controller was calibrated for the control of the temperature inside the glass container. Samples were loaded into the preheated chamber. The evaporation rate was evaluated by measuring the residual volume of the original solution containing PPy nanoparticles after a time interval. For fast evaporation (3.8×10^{-4}

* To whom correspondence should be addressed. Tel: 82-2-880-7069. Fax: 82-2-888-1604. E-mail: jsjang@plaza.snu.ac.kr.

(1) Deegan, R. D.; Bakajin, O.; Dupont, T. F.; Huber, G.; Nagel, S. R.; Witten, T. A. *Nature* **1997**, *389*, 827.
(2) Wickman, H. H.; Korley, J. N. *Nature* **1998**, *393*, 445.
(3) Sear, R. P.; Chung, S.-W.; Markovich, G.; Gelbart, W. M.; Heath, J. R. *Phys. Rev. E* **1999**, *59*, R6255.
(4) Okubo, T.; Kanayama, S.; Ogawa, H.; Hibino, M.; Kimura, K. *Colloid Polym. Sci.* **2004**, *282*, 230.
(5) Okubo, T.; Kimura, H.; Kawai, T.; Niimi, H. *Langmuir* **2003**, *19*, 6014.
(6) Okubo, T.; Okuda, S.; Kimura, H. *Colloid Polym. Sci.* **2002**, *280*, 454.
(7) Okubo, T.; Tsuchida, A.; Okuda, T.; Fujitsuna, K.; Ishikawa, M.; Morita, T.; Tada, T. *Colloids Surf., A* **1999**, *153*, 515.
(8) Shimomura, M.; Sawadaishi, T. *Curr. Opin. Colloid Interface Sci.* **2001**, *6*, 11.
(9) Karthaus, O.; Maruyama, N.; Cieren, X.; Shimomura, M.; Hasegawa, H.; Hashimoto, T. *Langmuir* **2000**, *16*, 6071.
(10) Ohara, P. C.; Heath, J. R.; Gelbart, W. M. *Angew. Chem., Int. Ed. Engl.* **1997**, *36*, 1077.
(11) Ohara, P. C.; Gelbart, W. M. *Langmuir* **1998**, *14*, 3418.
(12) Vossmeyer, T.; Chung, S.-W.; Gelbart, W. M.; Heath, J. R. *Adv. Mater.* **1998**, *10*, 351.
(13) Sellinger, A.; Weiss, P. M.; Nguyen, A.; Lu, Y.; Assink, R. A.; Gong, W.; Brinker, C. J. *Nature* **1998**, *394*, 256.
(14) Brinker, C. J.; Lu, Y.; Sellinger, A.; Fan, H. *Adv. Mater.* **1999**, *11*, 579.
(15) Lu, Y.; Fan, H.; Doke, N.; Loy, D. A.; Assink, R. A.; LaVan, D. A.; Brinker, C. J. *J. Am. Chem. Soc.* **2000**, *122*, 5258.
(16) Sommer, A. P.; Franke, R.-P. *Nano Lett.* **2003**, *3*, 574.
(17) Sommer, A. P.; Ben-Moshe, M.; Magdassi, S. *J. Phys. Chem. B* **2004**, *108*, 8.
(18) Jang, J.; Oh, J. H.; Stucky, G. D. *Angew. Chem., Int. Ed.* **2002**, *41*, 4016.
(19) Jang, J.; Oh, J. H. *Chem. Commun.* **2002**, 2200.

10.1021/la049259b CCC: $27.50
Published on Web 08/24/2004

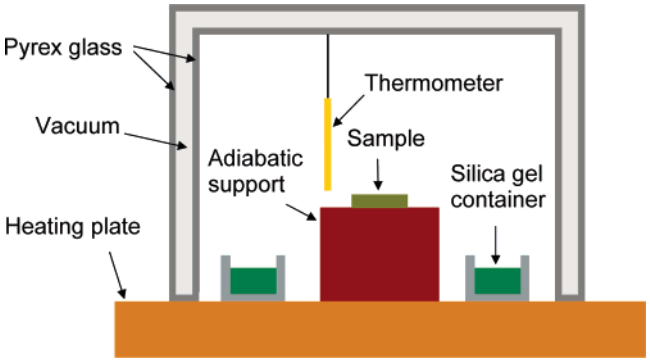

Figure 1. Schematic drawing of the evaporation system.

Scheme 1. Schematic Diagram for the Microemulsion Polymerization and the Formation of EISAs of PPy Nanoparticles

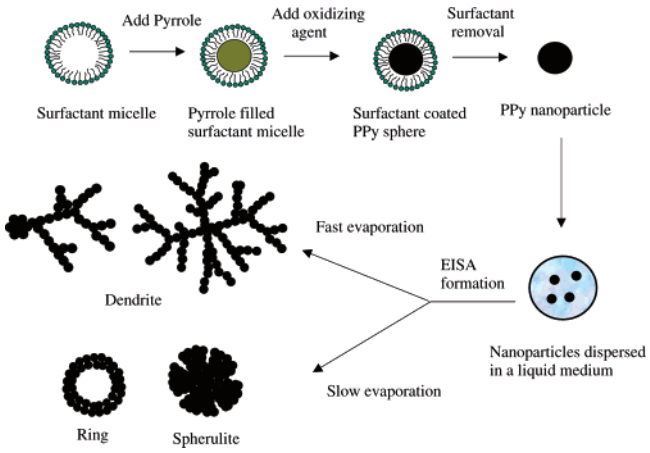

mL s^{-1}), the temperature inside the chamber was kept at 70 °C. On the contrary, the temperature was adjusted to 40 °C for slow evaporation (2.3×10^{-5} mL s^{-1}).

Two different types of carbon grids (a carbon film grid and a net-mesh carbon grid) were used as the solid substrate. The EISAs on the substrates were annealed at 120 °C for 3 h to make them robust. The surface roughness of solid substrates was measured with a Nanoscope IIIa Dimension 3100 SPM (Digital Instruments). Transmission electron microscope (TEM) images of EISAs were taken with a JEOL JEM-2000 FX microscope. The surface coverage of EISAs was analyzed by averaging the area fraction on the TEM images of 10 different copper meshes.

Results and Discussion

The overall experimental outline is illustrated in Scheme 1. Pyrrole monomers were introduced into the hydrophobic interior of microemulsion micelles and polymerized chemically at low temperature using ferric chloride as the oxidant. The low-temperature synthesis was appropriate for reducing the inner volume of a micelle due to the decreased surfactant chain mobility.[19] When the ultrasmall PPy particles were dispersed in ethyl alcohol, the isolated PPy nanoparticles were assembled spontaneously to form supramolecular structures during the solvent evaporation. The morphogenesis of EISAs was strongly related with the evaporation rate of the liquid medium and the nanoparticle concentration. Dendritic assemblies were observed in fast evaporation. In slow evaporation, ringlike patterns and spherulitic morphologies were observed. These phenomena result from the fact that the slow evaporation of the liquid medium endows the spherical particles with a well-ordered aggregate.[20] The root-mean-squared surface roughness of the carbon

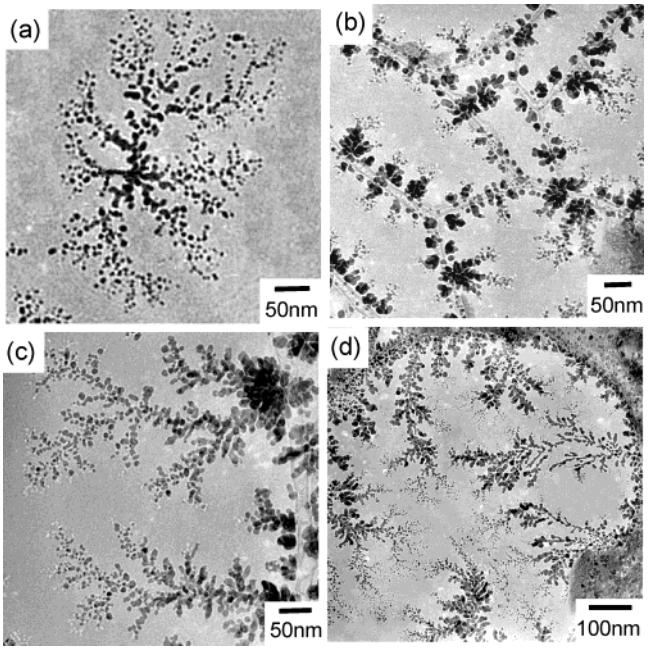

Figure 2. TEM images of (a) a 2-D dendrite formed on a carbon support film, (b) the initial stage of pseudo 1-D dendritic growth, (c) fully developed pseudo 1-D dendrites, and (d) pseudo 1-D dendrites formed from the solution containing a high concentration of nanoparticles (1.0 mg mL^{-1}) on a carbon net-mesh grid. The solvent evaporation rate was 3.8×10^{-4} mL s^{-1}, and the nanoparticle concentration except for image d was 0.085 mg mL^{-1}.

film substrate was 0.34 nm, which corresponds to about 1/15 of the average diameter of PPy nanoparticles. On the other hand, the carbon net-mesh grid consists of lacey carbon networks spread over copper meshes.

Figure 2a represents a TEM image of a dendrite formed on a carbon film grid at the solvent evaporation rate of 3.8×10^{-4} mL s^{-1}. The nanoparticle concentration was 0.085 mg mL^{-1}. PPy nanoparticles formed a nucleus first and tethered together from the core to make a dendritic array. In general, during the assembling process of colloidal particles, the coalesced nuclei of self-assemblies are known to be formed by long-range attractive interaction[2,21,22] and lateral capillary force (LCF)[23−25] of the colloidal particles.

While PPy chains can take positive charge owing to the presence of iron complex anion dopants, the overall surface charge of PPy nanoparticles can be considered to be almost neutral. Microemulsion polymerization increases the π-conjugation length and optimizes the arrangement of the molecular chains, thereby enhancing the hydrophobicity.[26] Therefore, the London dispersion force[27] can act on PPy nanoparticles. The magnitude of the dispersion force depends on the electronic frequency of the molecule. The attractive interaction arises because local fluctuations in the polarization within one particle induce a correlated response in the other via electromagnetic waves. The associated free energy decreases as the separation gets larger.

(20) Rakers, S.; Chi, L. F.; Fuchs, H. *Langmuir* **1997**, *13*, 7121.
(21) Hurd, A. J.; Schaefer, D. W. *Phys. Rev. Lett.* **1985**, *54*, 1043.
(22) Horvolgyi, Z.; Mate, M.; Zrinyi, M. *Colloids Surf., A* **1994**, *84*, 207.
(23) Denkov, N. D.; Velev, O. D.; Kralchevsky, P. A.; Ivanov, I. B.; Yoshimura, H.; Nagayama, K. *Nature* **1993**, *361*, 26.
(24) Denkov, N. D.; Velev, O. D.; Kralchevsky, P. A.; Ivanov, I. B.; Yoshimura, H.; Nagayama, K. *Langmuir* **1992**, *8*, 3183.
(25) Velev, O. D.; Denkov, N. D.; Paunov, V. N.; Kralchevsky, P. A.; Nagayama, K. *Langmuir* **1993**, *9*, 3702.
(26) Yan, F.; Xue, G.; Zhou, M. *J. Appl. Polym. Sci.* **2000**, *77*, 135.
(27) Israelachvili, J. N. *Intermolecular and Surface Forces*, 2nd ed.; Academic Press: London, 1991.

The LCF acts on particles protruding out of the liquid surface usually at the submonolayer level in which the thickness of the liquid layer approaches the diameter of the nanoparticles. Strong capillary forces arise owing to the meniscus formed between two particles. Their lateral projection drags the particles together, depending inversely on the particle distance. In our experimental conditions, the formation of the initial nucleus is considered to originate mainly from long-range attractive interactions. LCF becomes a dominant attractive interaction in the liquid level where the meniscus is clearly formed. In our experimental conditions, the LCF is unlikely to be exerted for the assembly of PPy nanoparticles with an average diameter of 5 nm, because the liquid film level should be very thin (about 2−3 nm thickness) for the LCF to be observed.[28]

In a later stage of the self-assembling process, remaining isolated nanoparticles are thought to be driven toward the nucleus by convective transport.[28,29] Convective transport arises from temperature gradients due to evaporative cooling. The liquid film spread on a core aggregate has a relatively thinner thickness and evaporates more rapidly. When the liquid evaporates, it has to be replaced by surrounding water. It is driven by the need to recover the local imbalance of the liquid level. The liquid flux toward the already existent aggregate moves further nanoparticles. Fast evaporation increases the convective force, resulting in the formation of fractal branches.

On the other hand, pseudo 1-D dendrites were formed on a net-mesh carbon grid at the same evaporation rate as the carbon film grid. Figure 2b,c exhibits the initial stage of dendritic growth (the image was taken without annealing) and the fully developed dendrite formed on a net-mesh carbon grid, respectively. The EISA could be formed despite the holes existing among the carbon networks. It is considered that an evaporating liquid film could be formed over the carbon networks owing to the strong surface tension of the liquid. The nucleation was observed mainly at the carbon meshes. While the nuclei forming in the liquid film vanished into the holes in the dried state, the nuclei forming in the carbon meshes could grow into a fully developed dendrite. In that case, the carbon mesh acted like a physical fence for the EISAs due to the larger height (15−25 nm thickness) of lacey carbon compared with the diameter of PPy nanoparticles and allowed pseudo 1-D dendritic growth of the fractal structures through heterogeneous nucleation. Figure 2d shows pseudo 1-D dendrites formed from higher concentration solution (1.0 mg mL^{-1}). Even though the nanoparticle concentration increased by about 12 times, the overall dimension of the pseudo one-dimensional dendrites was similar. On the contrary, the concentration of nanoparticles affected the surface coverage significantly. The surface coverage increased from about 20% to 45% when the concentration of nanoparticles was increased from 0.085 to 1.0 mg mL^{-1}. The reason is considered to be related to the increment of nucleation.

When the solvent evaporation rate was reduced from 3.8×10^{-4} to 2.3×10^{-5} mL s^{-1}, dendritic assemblies were not observed. Instead, ringlike assemblies and spherulitic compact aggregates formed. The size and shape of the EISAs in a slow evaporation were strongly dependent upon the nanoparticle concentration. Figure 3a displays ring assemblies formed on a carbon support film at the nanoparticle concentration of 1.0 mg mL^{-1}. The average diameter of ring patterns was about 50 nm. Intriguingly, the average diameter of ring patterns was enlarged from 50 to 180 nm by decreasing the nanoparticle concentration from 1.0 to 0.51 mg mL^{-1} (Figure 3b). On the other hand, when the nanoparticle concentration was diluted to 0.085 mg mL^{-1}, the ring morphologies disappeared and spherulitic assemblies were observed (Figure 3c).

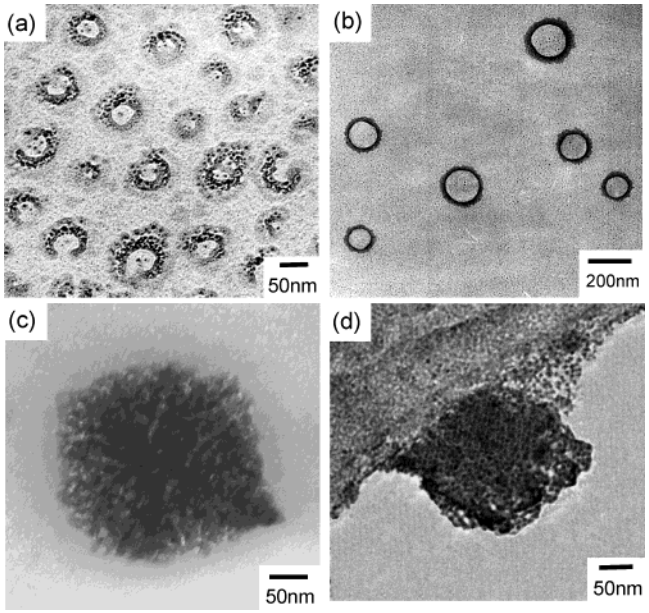

Figure 3. TEM images of EISAs observed at a low evaporation rate (2.3×10^{-5} mL s^{-1}). The size and shape of the EISAs on a carbon film grid were strongly dependent upon nanoparticle concentration: (a) small ring (1.0 mg mL^{-1}), (b) large ring (0.51 mg mL^{-1}), and (c) spherulitic compact structure (0.085 mg mL^{-1}). On a net-mesh grid, closely packed aggregates were only formed along the carbon meshes (d), irrespective of the nanoparticle concentration.

The hole opening phenomenon occurs in slowly evaporating wet films.[10,11] The hole opening pushes most PPy nanoparticles out along its advancing rim. In that case, isolated nanoparticles and their aggregates can protrude from the solvent film and feel frictional forces due to attraction toward the solid substrates. When the frictional force is high enough to prevent the nanoparticles from drifting, the pinning of the contact lines of nucleating holes occurs, resulting in a ring assembly. The PPy nanoparticles in a concentrated solution can be more easily pinned compared with the case of a dilute solution. On the contrary, the hole opening in a more dilute solution can be evolved further, which results in a retarded pinning of the contact lines. Therefore, the average diameter of ringlike assemblies increases with decreasing nanoparticle concentration. However, in the case of very low nanoparticle concentration, the growing holes are not pinned until they have run into one another. In that case, a closely packed aggregate emerges.

On the other hand, ring assemblies were not observed on a net-mesh grid. Irrespective of the nanoparticle concentration, closely packed aggregates were only observed on the carbon meshes (Figure 3d). The self-assemblies forming in the evaporating liquid film might vanish into the holes.

Table 1 presents a summary of the experimental data for the EISA morphologies obtained on a carbon film grid. Compared with conducting polymer particles, fractal structured conducting polymer assemblies are expected to show a percolation threshold at a lower filler content in their composite materials with an insulating polymer

(28) Xia, Y.; Gates, B.; Yin, Y.; Lu, Y. *Adv. Mater.* **2000**, *12*, 693.
(29) Lazarov, G. S.; Denkov, N. D.; Velev, O. D.; Kralchevsky, P. A.; Nagayama, K. *J. Chem. Soc., Faraday Trans.* **1994**, *90*, 2077.

Table 1. Summary of the EISA Morphologies Formed on Carbon Film Grid

EISA morphology	evaporation rate of liquid medium (mL s^{-1})	nanoparticle concentration (mg mL^{-1})	formation fraction on a substrate (%)
dendrite	3.8×10^{-4}	1.0	~45
	3.8×10^{-4}	8.5×10^{-2}	~20
small ring	2.3×10^{-5}	1.0	~50
large ring	2.3×10^{-5}	5.1×10^{-1}	~35
spherulite	2.3×10^{-5}	8.5×10^{-2}	~20

matrix. This is related to the effective formation of a conductive filler network in the composites using fractal structured conductive fillers.[30] In addition, a dendritic assembly is known to be applicable to an effective support material for catalysis owing to the large surface area.[31] The formation recipe of ring and spherulitic assemblies may possibly be introduced to the self-assemblies of other semiconducting nanoparticles for the purpose of tuning the electronic and optical properties. Importantly, these results may provide a guideline for the selective fabrication of EISA morphology and contribute to the understanding about the formation mechanism of EISAs using various nanoparticles.

Acknowledgment. This work has been supported by the BK 21 Program of the Korea Ministry of Education and by the Korea Science and Engineering Foundation through the Hyperstructured Organic Materials Research Center.

Supporting Information Available: The carbon film grid and an atomic force microscope image of the film surface; a schematic illustration of dendritic growth on a carbon support film at a high rate of solvent evaporation; a schematic explanation of dendritic growth on a carbon net-mesh grid at a high rate of solvent evaporation; a schematic representation of the formation mechanism of ring and spherulitic compact structures on a carbon net-mesh grid at a low rate of solvent evaporation; a schematic illustration of closely packed aggregates formed on a carbon net-mesh grid at a low rate of solvent evaporation; a schematic drawing of temperature gradients due to evaporative cooling; the method of determination of surface coverage of EISAs and average polydispersity in assembly size. This material is available free of charge via the Internet at http://pubs.acs.org.

LA049259B

(30) Shibuta, D. U.S. Patent 5,853,877, 1996.
(31) Zhou, Y.; Yu, S. H.; Wang, C. Y.; Li, X. G.; Zhu, Y. R.; Chen, Z. Y. *Adv. Mater.* **1999**, *11*, 850.